

Recent results of nucleon structure & matrix element calculations

Tanmoy Bhattacharya*, Rajan Gupta, and Boram Yoon

Los Alamos National Laboratory, Los Alamos, NM 87545, USA

E-mail: tanmoy@lanl.gov, rajan@lanl.gov, boram@lanl.gov

A review of recent lattice calculations of nucleon structure and matrix elements of operators in nucleons is presented. It primarily covers developments in the calculation of the matrix elements of the scalar, tensor, pseudo-scalar, axial-vector and vector operators in the ground state of neutrons and protons in the isospin symmetric limit. Some preliminary calculations of the electric dipole moment, the gravitational moments and stress-energy distribution, and the magnetic polarizability are briefly described.

37th International Symposium on Lattice Field Theory - Lattice2019

16-22 June 2019

Wuhan, China

*Speaker.

1. Introduction

This review will only cover the matrix elements of local, parity conserving, dimension-3, quark bilinears operators in the ground state of neutrons and protons in the isospin symmetric ($m_u = m_d$) limit. In particular, I will not discuss products or commutators of currents [1, 2, 3], contribution to the electric dipole moments from the QCD Θ -term [4], PDFs and their moments [5, 6], matrix elements within other baryon states [7], or decays [8], which are discussed by other speakers in these proceedings.

The calculational methodology of isovector matrix elements of nucleons is mature, however, control over all the systematics and assigning a reliable estimate of uncertainty to each needs to be reviewed. As discussed below, the errors in the scalar matrix elements are still large. There are new publications showing excited states with small mass gap contribute to isoscalar matrix elements at small nonzero momentum, *i.e.*, in the form factors, consequently the systematic error due to the excited state contamination may be underestimated. There has been no significant development in the methodology for reducing the systematics due to the renormalization factor, finite volume, discretization errors and scale-setting, and the chiral extrapolation to the light quark mass. Overall, the first part of my talk on nucleon charges has significant overlap with the recent FLAG 2019 report [9] that provides a status report up to the beginning of 2019, and the reader is referred to it.

2. Isovector g_A

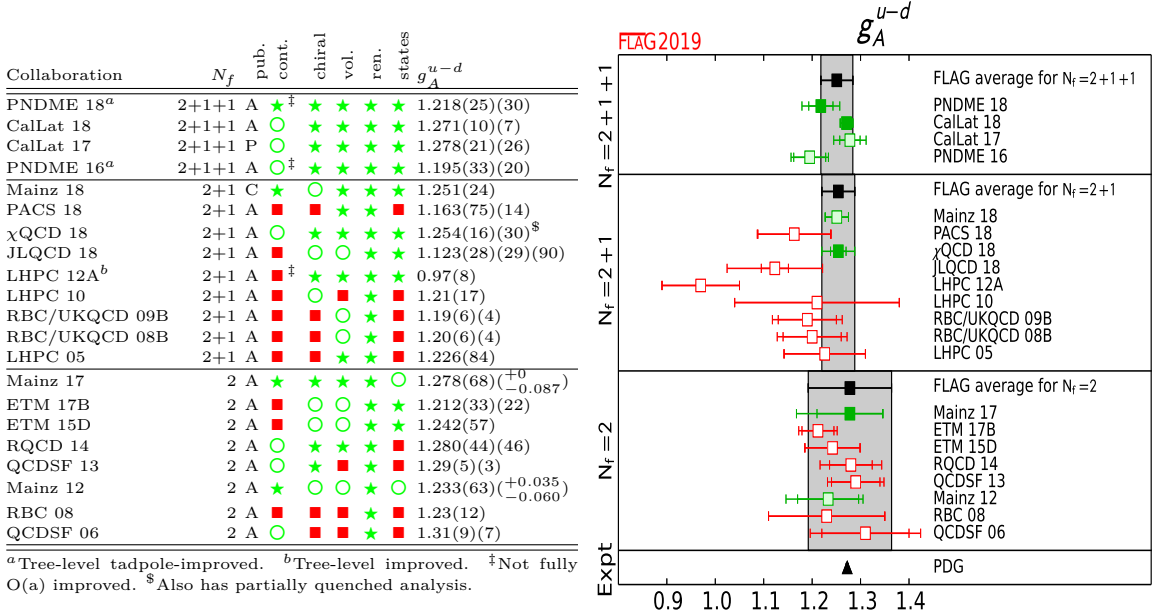


Figure 1: Compilation of the world data on isovector g_A presented in the FLAG [9] Review.

Fig. 1 from FLAG 2019 [9] gives the status of g_A^{u-d} and summarizes that calculations have obtained control at about the 3% level. Recent results from LHPC [10] using 2+1-flavor Clover fermions, RBC-UKQCD [11] using Domain Wall fermions at a lattice spacing

of 1.73 GeV, and by PNDME collaboration using Clover-on-Clover formulation with six 2+1 flavor clover fermions are consistent with this picture. In contrast, as shown in Fig. 2, the CalLat collaboration is claiming sub-percent accuracy [12]. The open question here is whether all the systematic effects, in particular excited states, are accounted for in their error estimate. The reservation is illustrated in Fig. 3. CalLat fit for g_A on the $a \approx 0.09$ fm, $M_\pi \approx 220$ MeV starts at $t \sim 3a$ and is dominated by the range $t/a = 3-8$, however, the two point function (M^{eff}) shows clear indication of excited states even up to $t \sim 10a$. In this regard, it is interesting to note the observation of the Mainz group [13] (See Fig. 4) that one needs to go out to about $1/2M_\pi$ before the lowest excited state mass expected from Chiral Perturbation theory [14] is manifest. If such low-mass states contribute to g_A , would it change the CalLat analysis based on small values of t , in particular the error estimate, *i.e.*, has the statistical precision been traded for unaccounted-for systematics? Is the CalLat analysis sensitive to possible low-lying excitations whose contribution is only expected to manifest at large time separations? Is the transition matrix element small? More work is needed to resolve these issues.

The ETMC collaboration [15] has compared various strategies for estimating the excited state contamination: the plateau method at large separations, the summation method, and using two-state fits. They quote results of the two-state fit, which covers the variation in the plateau values. Their results at the physical quark mass, but at a single value of $a \approx 0.08$ fm are consistent with the CalLat determination, but with about 1.5% errors. The ETMC result does not, however, include the $a \rightarrow 0$ extrapolation systematics. Lastly, the PACS collaboration has tested the efficacy of a Coulomb-gauge exponential source versus the usual Gaussian-smear sources in removing excited state contamination [16]. While the differences do not seem to be major, their latest statement is that the Gaussian-smear sources are better.

3. Isvector g_S and g_T

According to FLAG 2019 [9], the isovector $g_S = 1.022(80)(60)$ is currently known to about 10% and $g_T = 0.989(32)(10)$ to about 4%, see Figs. 5 and 6. New calculations presented in this conference from the LHPC [10], PACS [16], Mainz [13] and PNDME [17] collaborations agree with this consensus within one standard deviation. The ETMC collaboration [15] again finds that the two-state fits to remove excited state contributions resulted in the smallest statistical errors. Their results, 1.35(17), at a single lattice spacing of $a \approx 0.08$ fm differ from the world averages of the $a \rightarrow 0$ extrapolated values by about two standard deviations. Note, however, the systematic due to $a \rightarrow 0$ extrapolation in their estimate from this one ensemble is an unknown.

4. Flavor Diagonal Charges

Estimates for the flavor-diagonal charges have larger statistical and systematic uncertainty than the isovector case. Also, the connected and disconnected contributions are fit

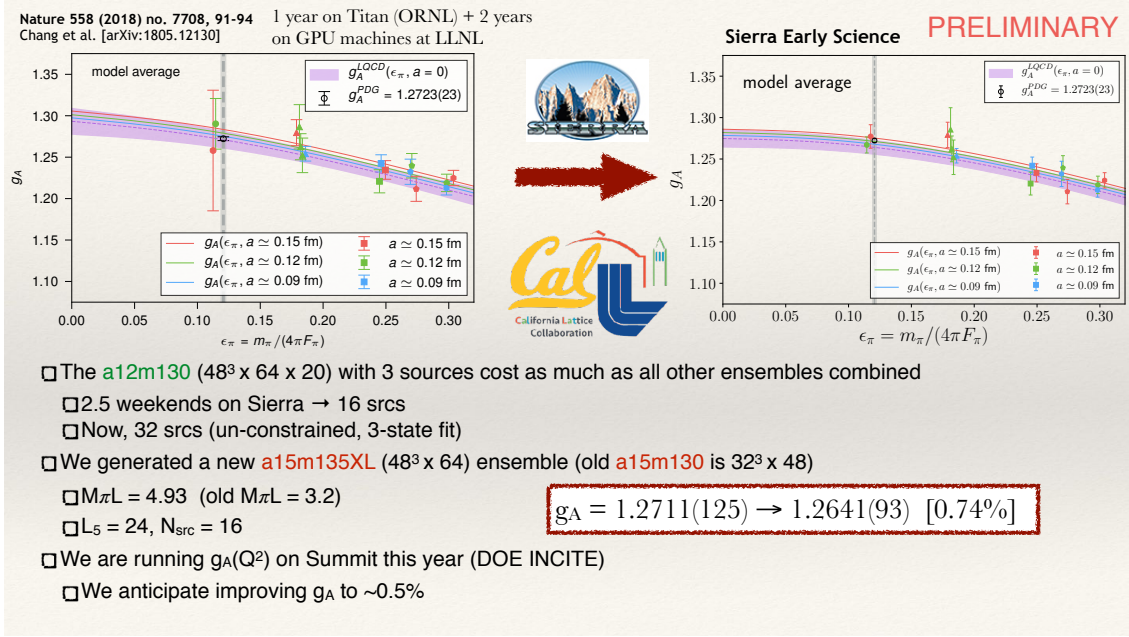


Figure 2: A slide from the CalLat [12] presentation explaining the improvements and expected reach of their calculations.

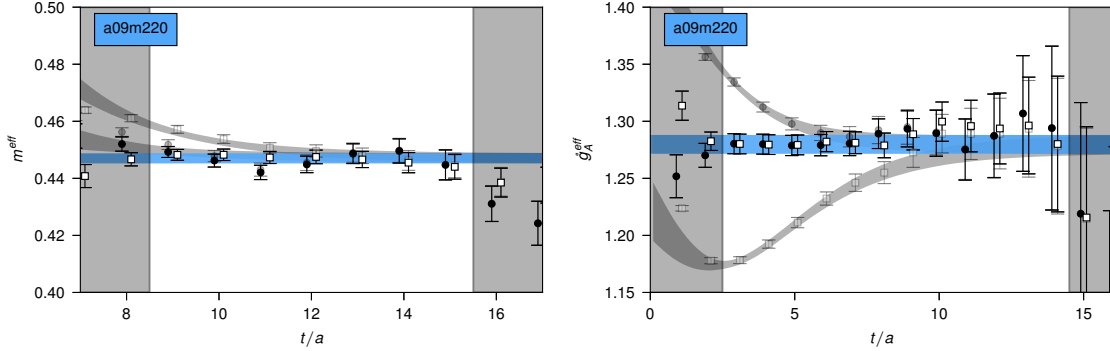


Figure 3: Effective mass plots for the extraction of the ground-state mass (left) and axial charge g_A (right) by the CalLat collaboration [12]. The extraction of the charge is dominated by the low error points at $t/a \approx 3$, the validity of which depends on reliable subtraction of excited states that clearly visible till $t/a \approx 10$.

separately (implying a partially quenched analysis) to remove the excited-state contamination [18]. The associated, presumably small, systematic is not estimated. As shown in Fig. 7, the u and d quark contributions, g_A^u and g_A^d are determined at the 5 and 8% accuracy. The difference is due to the fact that the magnitude of the d quark contribution is smaller but has a similar error. The much smaller strange quark contribution is known at 15% level. So far, very few collaborations have attempted to control all the systematics in the calculation of flavor diagonal charges, and a dependence on the sea charm quark cannot yet be ruled out. New results from the Mainz [13] and PNDME [17] collaboration

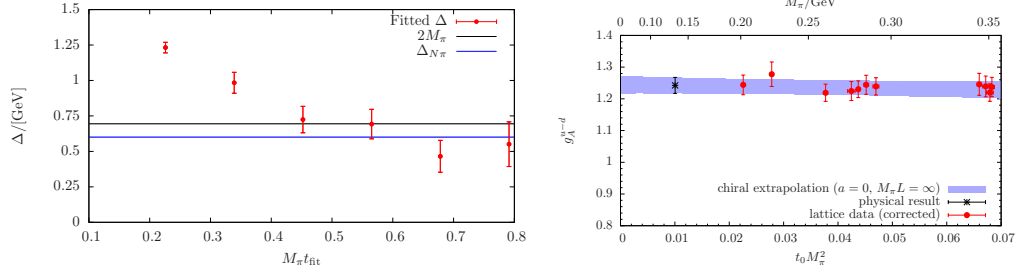


Figure 4: Calculation of the axial charge g_A by the Mainz collaboration [13]. The left panel shows an example of the determination of excited-state mass gap and the right panel shows the chiral extrapolation of their data. Chiral perturbation theory predicts the smallest mass gaps to be given by the horizontal lines, but the fitted mass gap is consistent with this only when they start at distances $M_\pi t_0 \approx 0.4$.

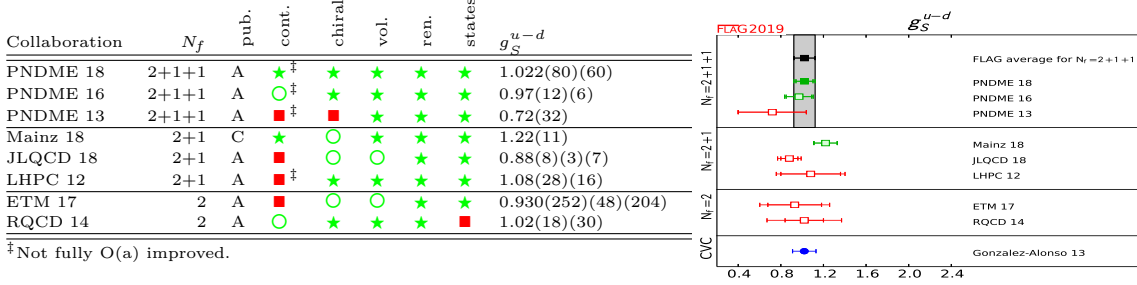


Figure 5: Compilation of the world data on isovector g_S presented in the FLAG [9] Review.

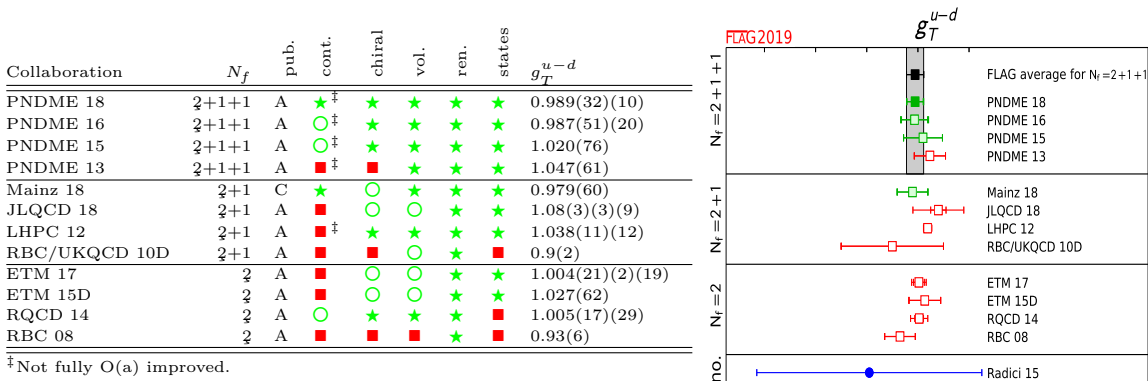


Figure 6: Compilation of the world data on isovector g_T presented in the FLAG [9] Review.

agree with the previous 2+1 and 2+1+1 results (FLAG averages), respectively.

The situation of the flavor-diagonal tensor charges is similar. As per the FLAG averages (Fig. 8), the u and d quark contributions are known at 4 and 7% accuracy, whereas the s quark contribution differs from zero only by 1.7σ . New calculations from the Mainz [19] and PNDME [17] collaborations give consistent values for the u and d quark contributions. PNDME have reduced the uncertainty on the s quark matrix element, g_T^s , and it is now negative with $> 2\sigma$ confidence.

Collaboration	N_f	pub.	cont.	chiral	vol.	ren.	states	Δu	Δd
PNDME 18A	2+1+1	A	★ [‡]	★	★	★	★	0.777(25)(30) [#]	-0.438(18)(30) [#]
χ QCD 18	2+1	A	○	★	★	★	★	0.847(18)(32) [§]	-0.407(16)(18) [§]
ETM 17C	2	A	■	○	○	★	★	0.830(26)(4)	-0.386(16)(6)
Δs									
PNDME 18A	2+1+1	A	★ [‡]	★	★	★	★	-0.053(8) [#]	
χ QCD 18	2+1	A	○	★	★	★	★	-0.035(6)(7) [§]	
JLQCD 18	2+1	A	■	○	○	★	★	-0.046(26)(9) [#]	
χ QCD 15	2+1	A	■	○	■	★	★	-0.0403(44)(78) [#]	
Engelhardt 12	2+1	A	■	○	○	★	★	-0.031(17) [#]	
ETM 17C	2	A	■	○	○	★	★	-0.042(10)(2)	

[#] $Z_A^{n,s} = Z_A^s$ assumed. [§] Also partially quenched analysis. [‡] Not fully O(a) improved.

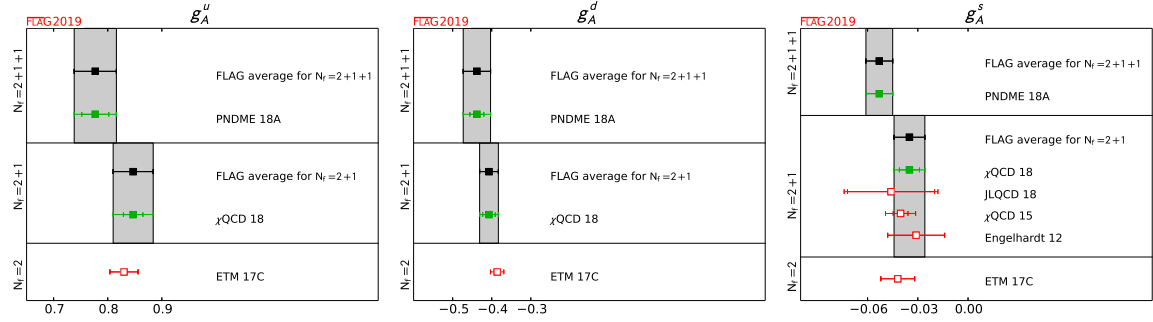


Figure 7: Compilation of the world data on flavor-diagonal g_A presented in the FLAG [9] Review.

The situation of the scalar charges that give the πN - σ term continues to be unresolved. As shown in Fig. 9, the $\sigma_{\pi N}$ results vary between a cluster around 40, and another around 60, with most controlled lattice calculations favoring the former. The 2+1+1 flavor average is the higher value, 65(13), coming from a single-ensemble calculation by the ETM collaboration [15] that includes the charm quark. The corresponding strange sigma term is known with about 20% accuracy, again preferring the smaller value of around 40 MeV. PNDME [17] has presented their first results favoring the smaller value of 34(6). They also report an additional systematic—a dependence on the renormalization scheme used. The RI-MOM scheme gives the smaller value, 23(7) compared to the RI-SMOM. This scheme dependence needs further attention.

The BMW collaboration [20] presented preliminary results for the nucleon sigma terms for the u , d , s and c quarks using a stout staggered action. The values for σ_{qN} are consistent with their earlier results.

5. Vector Form Factor

The quantity of highest phenomenological interest for the vector and axial form factors

Collaboration	N_f	pub.	cont.	chiral	vol.	ren.	states	g_T^u	g_T^d
PNDME 18B	2+1+1	P	★ [‡]	★	★	★	★	0.784(28)(10) [#]	-0.204(11)(10) [#]
PNDME 16	2+1+1	A	○ [‡]	★	★	★	★	0.792(42) ^{#&}	-0.194(14) ^{#&}
PNDME 15	2+1+1	A	○ [‡]	★	★	★	★	0.774(66) [#]	-0.233(28) [#]
JLQCD 18	2+1	A	■	○	○	★	★	0.85(3)(2)(7)	-0.24(2)(0)(2)
ETM 17	2	A	■	○	○	★	★	0.782(16)(2)(13)	-0.219(10)(2)(13)
g_T^s									
PNDME 18B	2+1+1	P	★ [‡]	★	★	★	★	-0.0027(16) [#]	
PNDME 15	2+1+1	A	○ [‡]	★	★	★	★	0.008(9) [#]	
JLQCD 18	2+1	A	■	○	○	★	★	-0.012(16)(8)	
ETM 17	2	A	■	○	○	★	★	-0.00319(69)(2)(22)	

[#] $Z_T^{n..s.} = Z_T^s$ assumed. [&] Only 'connected'. [‡] Not fully O(a) improved.

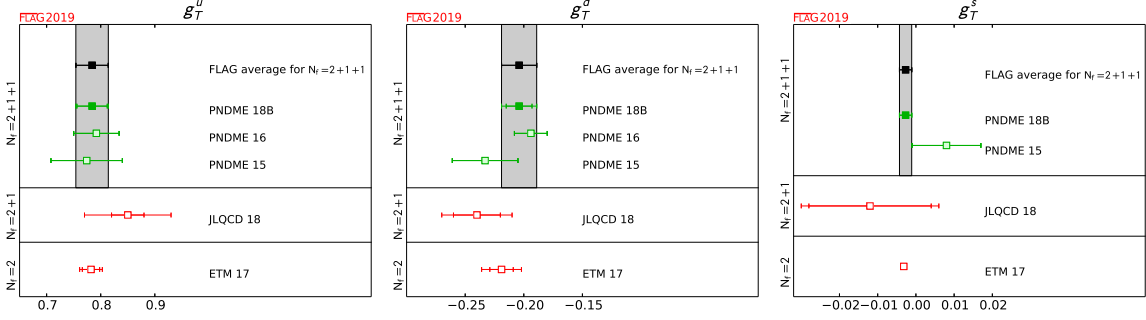


Figure 8: Compilation of the world data on flavor-diagonal g_T presented in the FLAG [9] Review.

is their momentum dependence over a range of Q^2 values. The matrix elements of the vector current are, in general, parameterized in terms of four form-factors, $F_{1,2,A,3}(Q^2)$. Of these, F_A and F_3 are zero when parity is a good symmetry, and the F_1 and F_2 are usually combined into the electric and magnetic form-factors G_E and G_M that have a clear interpretation in the Breit frame:

$$\langle N|V_\mu|N\rangle \equiv \bar{u} \left[F_1 \gamma_\mu + F_2 \sigma_{\mu\nu} \frac{q_\nu}{2M} + F_A \frac{2iMq_\mu - q^2 \gamma_\mu}{m_N^2} \gamma_5 - iF_3 \sigma_{\mu\nu} \frac{q_\nu}{2M} \gamma_5 \right] u$$

$$G_E = F_1 - \frac{Q^2}{4M^2} F_2 \quad G_M = F_1 + F_2$$

The experimental values of these form-factors are very well parameterized by the Kelly curve, so it was disconcerting that the lattice data for G_E (from simulations with $M_\pi < 150$ MeV) lie systematically above the curve at $Q^2 > 0.1$ GeV², as shown in the upper panels in Fig. 10 taken from Ref. [21]. The G_M data, on the other hand, tend to fall below the curve for $Q^2 < 0.1$ GeV². The large-volume data from the PACS collaboration [22], is an exception, and tends to lie closer to the phenomenological results, but are based on very low statistics. As shown in Tab. 1, the isovector magnetic moment $\mu = G_M(0)/G_E(0) \equiv \mu^p - \mu^n$, and the electromagnetic radii, $\langle r_{E,M}^2 \equiv -6 \frac{d}{dQ^2} \left(\frac{G_{E,M}(Q^2)}{G_{E,M}(0)} \right) \Big|_{Q^2=0}$ determined on the lattice also deviate from their phenomenological estimates.

The analysis by the PNDME [21] also shows that the lattice results are much closer to the Kelly determination if the scale is set from the nucleon mass as shown in the lower two panels in Fig. 10. The magnitude of the remaining disagreement is comparable to the scale-setting uncertainty, and points to an underestimate of the extrapolation systematics as a likely cause.

The new results presented by the PNDME collaboration [17] using the Clover-on-Clover data (See Fig. 11) show much better agreement with the Kelly curve than the Clover-on-

Collaboration	N_f	pub.	cont.	chiral	vol.	ren.	states	$\sigma_{\pi N}$ [MeV]	σ_s [MeV]
MILC 12C	2+1+1	A	★	★	★	★	—	0.44(8)(5) $\times m_s^{\text{¶}\S}$	—
JLQCD 18	2+1	A	■	○	○	★	26(3)(5)(2)	17(18)(9)	—
χ QCD 15A	2+1	A	○	★	★	★	45.9(7.4)(2.8) [§]	40.2(11.7)(3.5) [§]	—
χ QCD 13A	2+1	A	○	★	○	★	—	33.3(6.2) [§]	—
JLQCD 12A	2+1	A	■	○	○	★	—	0.009(15)(16) $\times m_N^\dagger$	—
Engelhardt 12	2+1	A	■	○	■	★	—	0.046(11) $\times m_N^\dagger$	—
MILC 12C	2+1	A	★	○	★	★	—	0.637(55)(74) $\times m_s^{\text{¶}\S}$	—
MILC 09D	2+1	A	★	○	★	★	—	59(6)(8) [§]	—
ETM 16A	2	A	■	○	○	★	37.2(2.6) ^(4,7) _(2,9)	41.1(8.2) ^(7,8) _(5,8)	—
RQCD 16	2	A	○	★	★	■	35(6)	35(12)	—
ETM 14A	2+1+1	A	★	○	○	—	64.9(1.5)(13.2) ^{\Delta}	—	—
BMW 15	2+1	A	★ [‡]	★	★	—	38(3)(3)	105(41)(37)	—
Junnarkar 13	2+1	A	○	○	○	—	—	48(10)(15)	—
Shanahan 12	2+1	A	■	○	○	—	45(6)/51(7) [*]	21(6)/59(6) [*]	—
JLQCD 12A	2+1	A	■	○	○	—	—	0.023(29)(28) $\times m_N^\dagger$	—
QCDSF 11	2+1	A	○	■	○	—	31(3)(4)	71(34)(59)	—
BMW 11A	2+1	A	○ [‡]	★	○	—	39(4) ⁽¹⁸⁾ ₍₇₎	67(27) ⁽⁵⁵⁾ ₍₄₇₎	—
Martin Camalich 10	2+1	A	■	★	■	—	59(2)(17)	-4(23)(25)	—
PACS-CS 09	2+1	A	■	★	○	—	75(15)	—	—
QCDSF 12	2	A	○	★	○	—	37(8)(6)	—	—
JLQCD 08B	2	A	■	○	■	—	53(2) ⁽⁺²¹⁾ ₍₋₇₎	—	—

^{\Delta} Multiple results. [‡] Not fully O(a) improved. ^{*} Two results are quoted. [†] From $f_{T_s} = \sigma_s/m_N$ [§] Also partially quenched [¶] At $\mu = 2$ GeV in $\overline{\text{MS}}$ scheme.

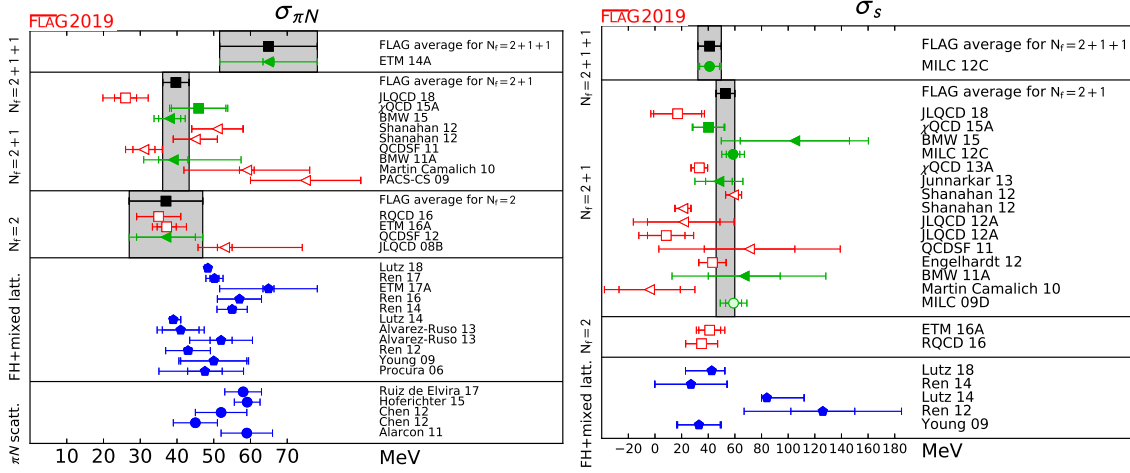


Figure 9: Compilation of the world data on isosinglet g_S presented in the FLAG [9] Review.

HISQ data for both G_E and G_M . The reason for the improvement with respect to previous results has not been identified, so further assessment of the systematics needs to be carried out.

New results for the disconnected contributions to the form-factors are available from the ETMC [23] and Mainz [19] collaborations (See Figs. 13 and 12). The strange electromagnetic radii and magnetic moment are still determined poorly: they are within 2 standard errors of zero if statistical and systematic errors are added in quadrature. More importantly for this discussion, inclusion of these do not resolve the disagreement with the experimental results. Furthermore, the lattice data do not show the enhancement of the electric form-factor around 0.2 GeV^2 as seen in some experimental data.

6. Axial Form Factor

The situation for the axial form factors has been much more questionable as previous

	M_N MeV	a from	Q^2 Fit	r_E (fm)	r_M (fm)	μ
PNDME	953(4)	r_1	z^4	0.769(40)	0.671(90)	3.94(17)
PNDME a06	951(10)	r_1	z^4	0.765(14)	0.704(36)	3.98(15)
LHPC'17	912(8)	M_Ω	z^5	0.887(49)		4.75(15)
ETMC'18	929(6)	r_0	dipole	0.802(22)	0.714(93)	3.96(16)
ETMC'17	941(2)	r_0	dipole	0.808(36)	0.732(58)	4.02(35)
PACS'18	958(10)	M_Ω	$z^8 z^7$	0.915(99)	1.437(409)	4.81(79)
PACS'18A	942(11)	M_Ω	dipole	0.875(32)	0.805(276)	4.42(35)

Table 1: The values of the neutron magnetic moment, and the electromagnetic charge radii from the various collaborations. Various quoted errors have been added in quadrature. Experimentally, $\mu^p = 1.79$, $\mu^n = -1.91$, $r_E = 0.875(6)$ from electrons and $0.8409(4)$ from muons.

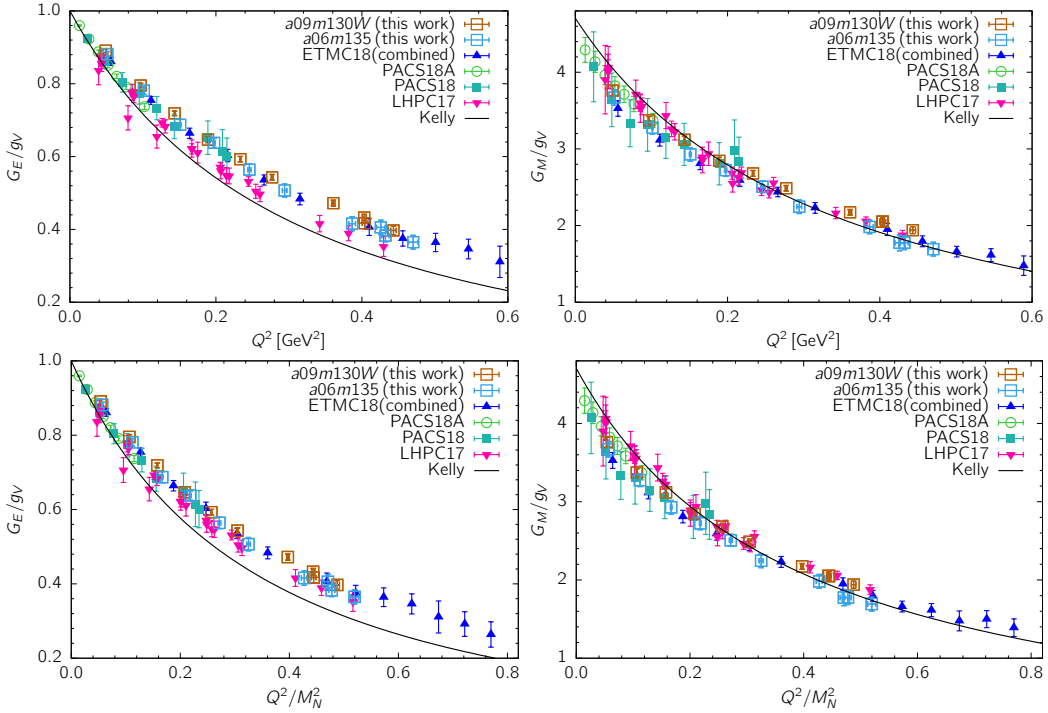


Figure 10: World data for the electric and magnetic form factors G_E and G_M from simulations with $M_\pi < 150$ MeV compiled in Ref. [21]. The upper two panels show the data plotted versus Q^2 and the lower panels versus Q^2/M_N^2 . The difference is due to what quantity is used to set the lattice scale, and is indicative of discretization errors.

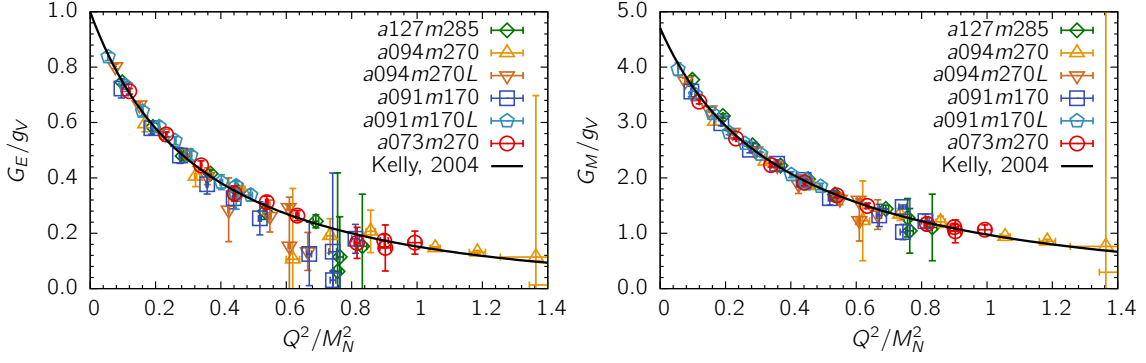
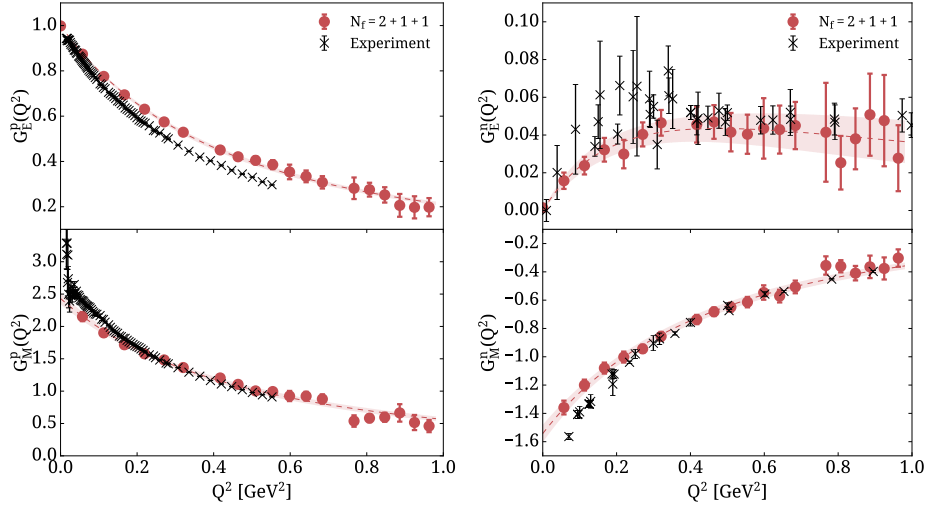


Figure 11: New results on the electromagnetic form factors from the PNDME collaboration [17].

Proton and neutron electric and magnetic form factors

Extended Twisted Mass collaboration using $N_f = 2 + 1 + 1$ simulations at the physical point, with $a = 0.08$ fm and $64^3 \times 128$ lattice



Deviations from experimental results under investigation. // May arise from e.g. finite volume and/or excited states

C. A., S. Bacchio, M. Constantinou, J. Finkenrath, K. Hadjiyiannakou, K. Jansen, G. Koutsou and A. Vaquero Aviles-Casco, arXiv:1812.10311.

Nucleon structure

3 / 3

Figure 12: Slide from the ETM collaboration showing the results [23] for the electric and magnetic form-factors of the proton including disconnected contributions.

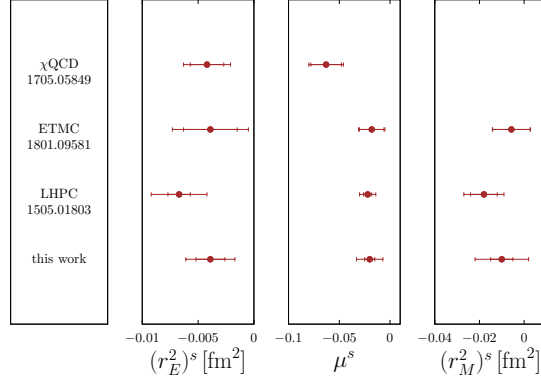
results violated the PCAC relation. The axial form factors are defined by

$$\langle N | A_\mu | N \rangle \equiv \bar{u} \left[G_A \gamma_\mu + \tilde{G}_P \frac{q_\mu}{2M} \right] \gamma_5 u \quad (6.1)$$

$$\langle N | P | N \rangle \equiv \bar{u} G_P \gamma_5 u \quad (6.2)$$

From these, the axial radius is extracted using

$$\langle r_A^2 \rangle \equiv -6 \frac{d}{dQ^2} \left(\frac{G_A(Q^2)}{G_A(0)} \right) \Big|_{Q^2=0} \quad (6.3)$$



$$\begin{aligned} (r_E^2)^s &= -0.0039(13)(18) \text{ fm}^2 \\ \mu^s &= -0.020(5)(12) \\ (r_M^2)^s &= -0.010(5)(11) \text{ fm}^2 \end{aligned}$$

Figure 13: Slide from the Mainz collaboration [19] displaying the comparison of their results for the strange contribution to the nucleon with previous results.

Neutrino scattering data pre-2000 were fit to a dipole form to obtain $r_A = 0.666(17)$ fm and a dipole mass of $M_A = 1.026(21)$ GeV [24], which agrees with those obtained from the recent analysis of the deuterium system using the z -expansion: $r_A = 0.68(16)$ fm and $M_A = 1.00(24)$ GeV [25]. The latter, however, has much larger uncertainty, which the authors contend is more realistic. On the other hand, the MiniBooNE Collaboration, using the dipole ansatz and a relativistic Fermi gas model [26, 27], find that $M_A = 1.35(17)$ GeV reproduces their double differential cross section for charged current quasi-elastic neutrino and antineutrino scattering off carbon [28]. Thus, one needs to resolve three questions: (i) Is the dipole ansatz a good approximation to the Q^2 behavior? (ii) If it is, what is the value of M_A ? And, (iii) the cause and resolution of the observation violation of PCAC in the lattice data discussed below.

The 2017 PNDME lattice results [29], shown in Figure 14, lie closer to the data from the MiniBooNE experiment. In fact a dipole fit gives $r_A = 0.505(13)(6)$ fm and $M_A = 1.35(3)(2)$ GeV. A z -expansion fit gives an even smaller slope at the origin: $r_A = 0.481(58)(62)$ fm and $M_A = 1.42(17)(18)$ GeV. Their main conclusion was that the data show little variation versus the lattice spacing a and the pion mass M_π , however, to extract r_A , more data near $Q^2 = 0$ are needed. Results from the ETMC collaboration were similar and gave $M_A = 1.322(42)(17)$ GeV [30].

New results on the disconnected contribution, in particular the strange contribution, were also presented this year by the Mainz collaboration [19].

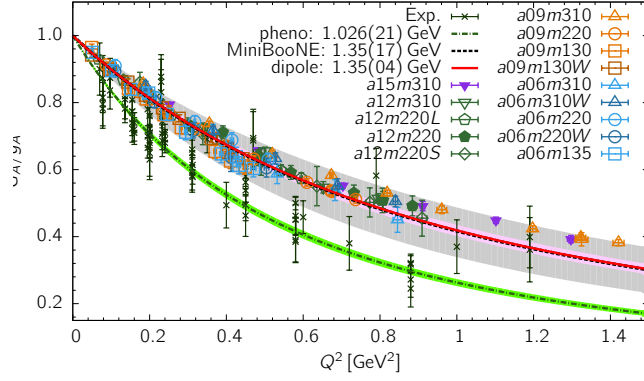


Figure 14: Results from the PNDME collaboration on the axial form factors.

7. PCAC Relation

A major advance this year was a credible resolution to the violation of the PCAC relation on the lattice [31]. The situation previously could be summarized as: even though the Axial Ward Identity: $\partial_\mu A^\mu = 2\hat{m}P$ was indeed satisfied by the correlation functions on the lattice, the corresponding relation between the extracted form-factor written as $(R_1 \equiv \frac{2\hat{m}G_P}{2MG_A} 2MG_A) + (R_2 \equiv \frac{Q^2\tilde{G}_P}{4M_N^2G_A}) = 1$ was strongly violated. These violations grew as $M_\pi \rightarrow 0$ and $Q^2 \rightarrow 0$. In addition, the related hypothesis of pion-pole dominance, $R_4 \equiv \frac{4\hat{m}M_N G_P}{M_\pi^2 G_P} = 1$ was equally badly violated [29]. This is illustrated in Fig. 15, where we also plot the combination $R_3 \equiv \frac{(Q^2 + M_\pi^2)\tilde{G}_P}{4M_N^2 G_A} = 1$, and R_5 , the expected $O(a)$ correction to R_1 calculated with the the unimproved axial current.

Bali *et al.* [32] proposed a fix for this using projected currents $A_\mu^\perp = (g_{\mu\nu} - \bar{p}_\mu \bar{p}_\nu / \bar{p}^2) A_\nu$, with 4-momentum \bar{p} the reflection of p about the light cone. The diagonal matrix element of the added term should be zero in any spin-half state, so this current should provide an equally good determination of the axial form-factors of the neutron, but possibly removing excited state effect due to transition matrix elements. They then suggested shifting the pseudoscalar operator by a similar term, $P^\perp = P - (\frac{1}{2im_q} \bar{p}_\mu \bar{p}_\nu / \bar{p}^2) \partial_\mu A_\nu$ but enforcing $p^\mu A_\mu^\perp = 2\hat{m}P^\perp$. The matrix element of P^\perp was much larger and helped satisfy PCAC. Since the quark masses m_q are small numbers, it was *a priori* unclear whether the large shift could be caused merely by $O(a^2)$ effects being amplified by the smallness of the quark mass. Also, it was not clear why this projection was needed in the first place. Lastly, this construct did not fix the small value of g_p^* . An interesting feature of this proposed solution is that the projection almost completely eliminates contributions from the A_4 , and its large excited state effect, instead A_4^\perp is dominated by contributions from A_i .

The PNDME collaboration, on the other hand showed [33] that the problem is resolved by including low-mass excited states when removing the excited state contamination, and the matrix element of the A_4 current is key to their solution. In particular, when the mass-gap between the first-excited and the ground-state is extracted from the two-point function, the matrix elements of the spatial components A_i are well-fit, but the matrix

elements of A_4 has very large χ^2 . These latter matrix elements can, however, be fit if the mass-gap is left free (see Fig. 16). The fit value of the mass-gap is close to a non-interacting intermediate $N\pi$ state. It is much smaller but cannot be ruled out by fits to the two-point fit on the basis of χ^2 . The A_i correlators, on the other hand, fit equally well with any of these mass-gaps, but the extrapolated results turn out to be different. What PNDME finds (see Fig. 17) is that using the much smaller mass-gap, the PCAC relation, as well as the pion pole-dominance (g_P^*), are satisfied up to small corrections that are of size that can plausibly be attributed to $O(a)$ effects.

The net outcome is a new determination of the form factors G_A , G_P and \tilde{G}_P . They present results for both the Clover-on-HISQ [33] and Clover-on-Clover [17] analysis. The results of the two analysis are similar: the latter results are reproduced here in Fig. 18.

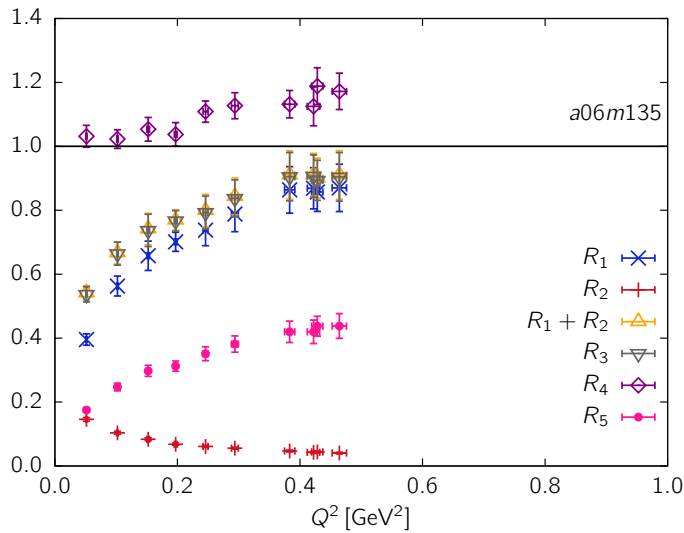


Figure 15: Various ratios of extracted form factors describing the violation of PCAC.

8. Other matrix elements

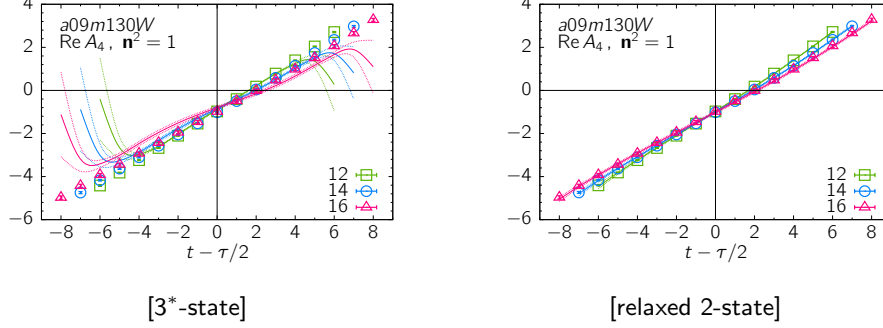
In this section, we briefly comment on the recent advances in calculating the nucleon matrix elements of a few other operators. These calculations are all preliminary—often the first calculations of their nature on the lattice—and the systematics are yet to be controlled.

8.1 CP violation from BSM

The calculation of nEDM due to the Θ -term is discussed in the plenary lecture by H. Ohki [4]. Last year also saw a lot of activity in the calculation of the neutron EDM arising from the operators beyond the standard model, especially those due to the quark chromo-EDM and the Weinberg operator. In a parallel talk, Boram Yoon [34], summarized the unrenormalized results for the F_3 form factors, which are reproduced in Fig. 19. As

Axial Current A_4 3-pt Correlator

[arXiv:1905.06470]



- E_i, \mathcal{A}'_i and M_j, \mathcal{A}_j are taken from 4-state fits to nucleon two-point correlator. ($i, j = 0, 1, 2$)

- E_0, \mathcal{A}'_0 and M_0, \mathcal{A}_0 are taken from nucleon two-point correlator fits. Excited state parameters are free.

n^2	3*-state		relaxed 2-state	
	$\chi^2/\text{d.o.f}$	p -value	$\chi^2/\text{d.o.f}$	p -value
1	21.78	$< 5 \times 10^{-5}$	0.698	0.76
2	19.36	$< 5 \times 10^{-5}$	1.654	0.06
3	11.79	$< 5 \times 10^{-5}$	2.018	0.02

Figure 16: Slide from PNDME [33] showing fits to the A_4 correlation function showing that the mass-gap determined from the two-point function does not fit the A_4 correlator (top left), but leaving it free gives a good fit (top right). The bottom table provides the χ^2 values for the different fits.

PCAC with Excited States ($N\pi$) from A_4

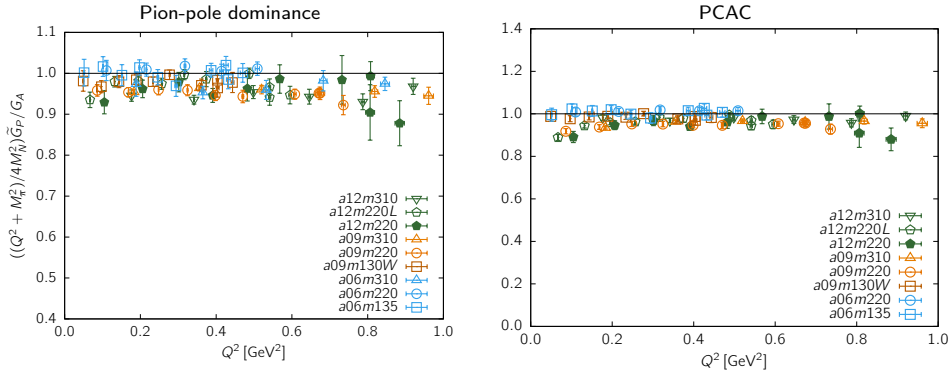


Figure 17: Slide from PNDME [33] claiming solution to the PCAC puzzle in terms of a low-lying excited state that had been missed. Both the ratios measuring violation of pion-pole dominance (left) and of PCAC relation between form factors (right) are unity if the low-lying excited state is accounted for.

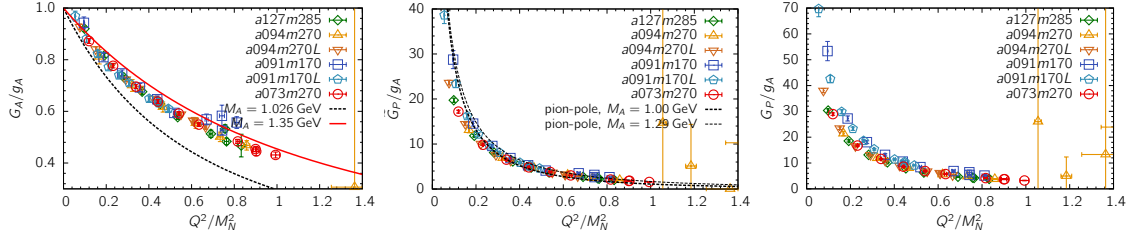


Figure 18: Isovector form-factors G_A , \tilde{G}_P and G_P obtained by the PNDME collaboration [17] taking into account the low-lying $N\pi$ excited state contamination.

can be seen, the statistical errors in the case of the Weinberg operator are not yet under control. For the quark chromo-EDM, the data from different groups using different actions, naively show a very large quark-mass dependence. Further analysis is needed to understand whether the renormalization and operator mixing effects can explain this.

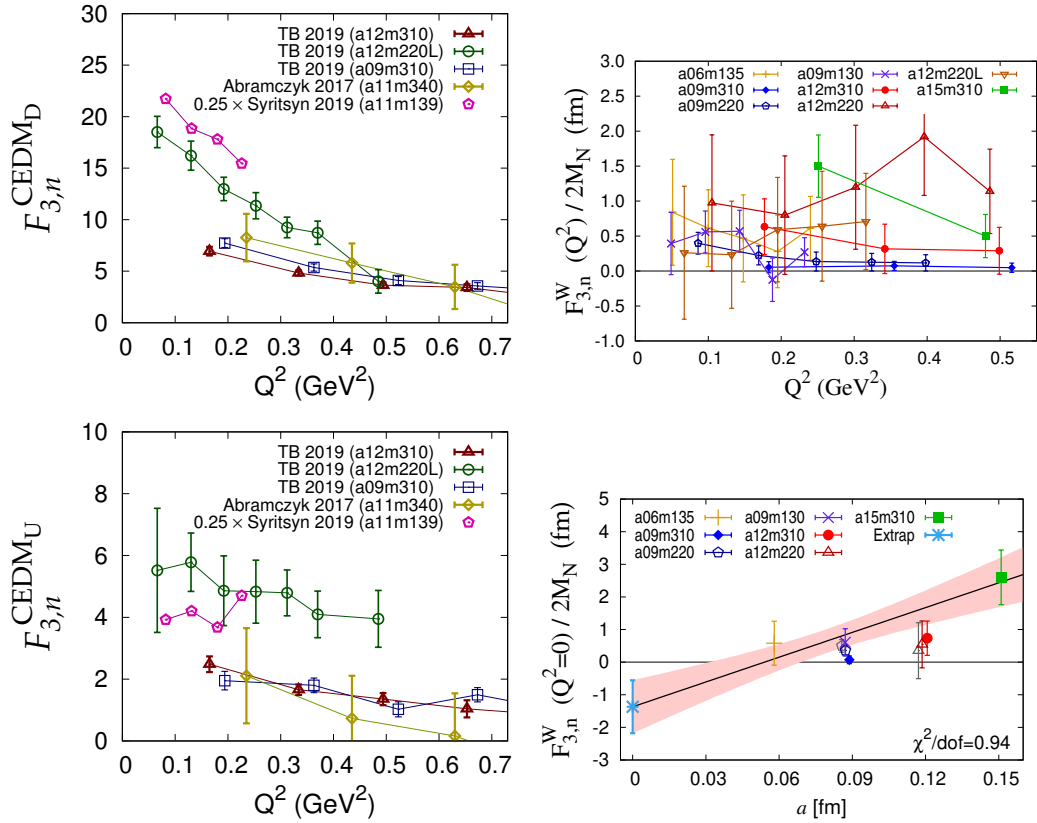


Figure 19: Comparison of the extraction of the electric dipole moment of the nucleon from the chromo-EDM and the Weinberg three-gluon operators, taken from the talk by B. Yoon [34]. Only connected diagrams have been calculated, and the data shown are the lattice numbers without any renormalization.

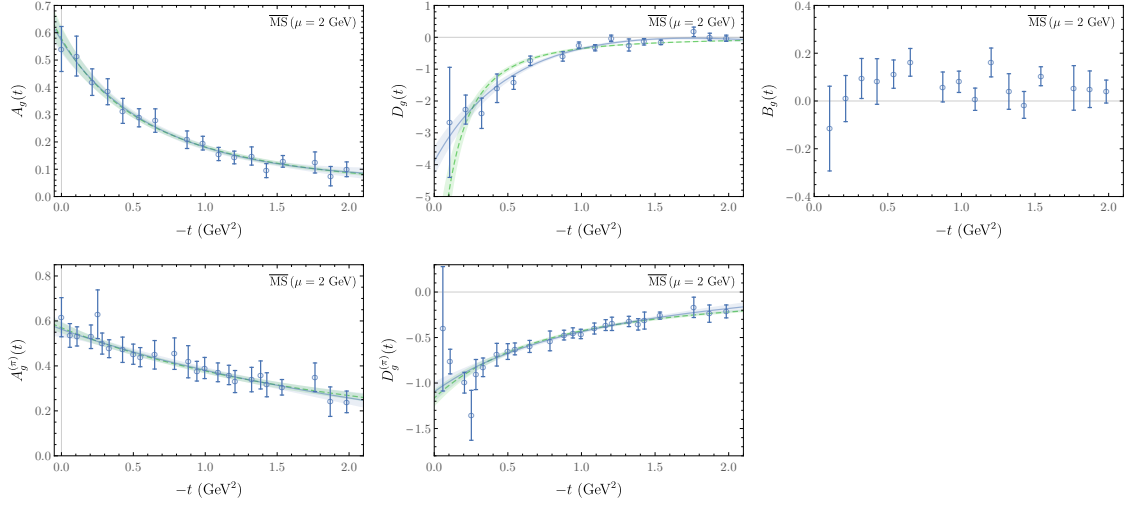


Figure 20: The gravitational moments of the nucleon by Shanahan and Detmold [35].

8.2 Gravitational Moments

In the last year, Shanahan and Detmold have provided the first calculations [35, 36] of the gravitational moment of the nucleon (Fig. 20) and the pressure and shear distribution within the nucleon (Fig. 21). These calculations have been done with a large pion mass ensemble, but provide the first estimate of the mechanical radius of the proton as $0.71(1)$ fm. Their data for the pressure and shear distributions, when fit using model-independent z -fits, have large errors, and the systematics need further study.

8.3 Magnetic Polarizability

First results on calculating the polarizability of the nucleon were presented by the Adelaide collaboration [37], and are reproduced here as Fig. 22. These first calculations need further study before the systematics, especially the chiral extrapolation, is understood.

9. Future

The lessons from these calculations is that though lattice calculations have matured, we still need to improve our approach to understanding systematic errors. In particular, it is easy to inadvertently increase the systematic errors in our quest to reduce systematic errors. In particular, the question that we need to ask is not whether any systematic is visible in a given data set, but, rather, how *large* a systematic could be masked in it. The approach advocated by a number of groups that use model averaging is a step in the right direction, but does not solve the problem since the space of models averaged may not be large enough, and the weights assigned to the conservative models may be too low. Partial solution would be to move over to properly chosen blind analysis techniques, since, at least, unconscious bias gets minimized in such approaches.

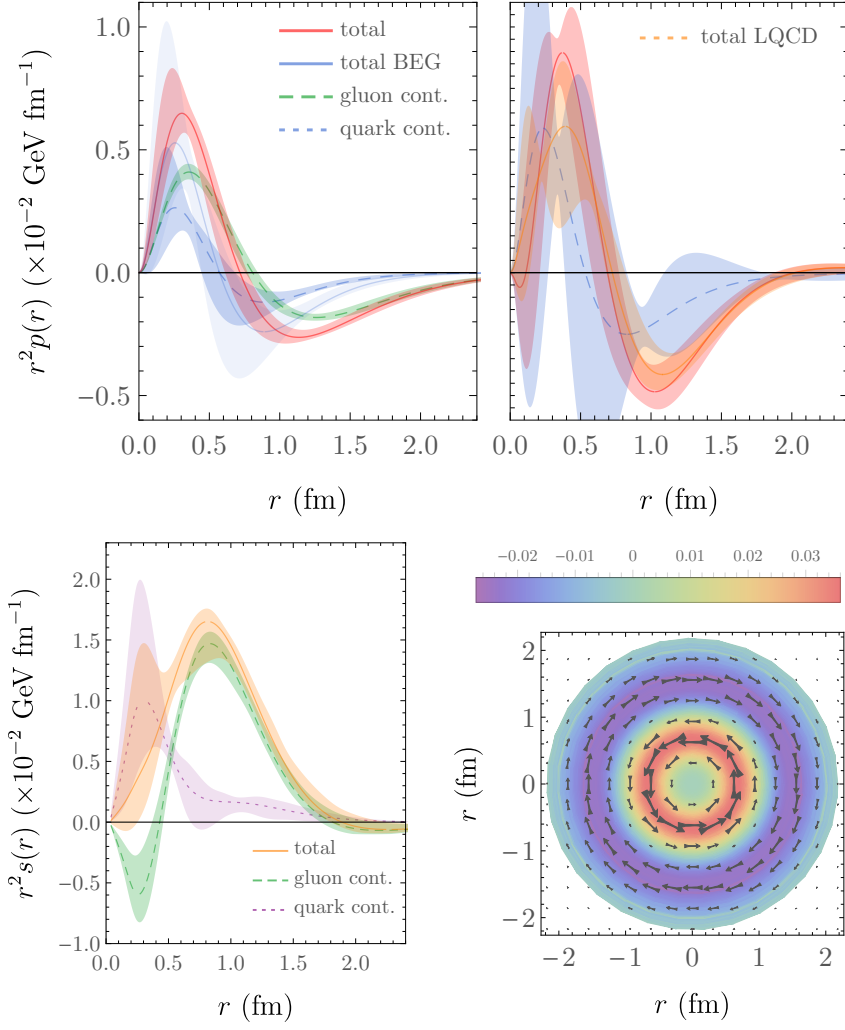


Figure 21: Pressure and shear distribution inside the nucleon by Shanahan and Detmold [36].

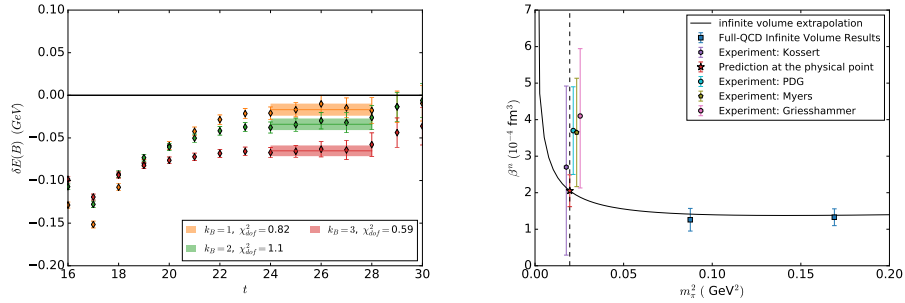


Figure 22: Magnetic polarizability of the nucleon [37].

There are still many operators, calculating whose matrix elements needs more work. We need a better control (statistical and systematic) of disconnected diagrams, of scalar matrix elements, as well as matrix elements of higher dimensional (BSM) operators.

10. Acknowledgments

Thanks to Yong-chull Jang for help with the presentation. I would also like to thank everybody that sent me unpublished materials or drew my attention to their work. For the data from our own collaborations, I would like to thank OLCF, NERSC, USQCD for computer allocations allowing these calculations, MILC Collaboration for HISQ lattices, and LANL LDRD and DOE office of science for supporting this research and me.

References

- [1] C. Zimmermann on behalf of the RQCD Collaboration. “Two-current correlations and DPDs for the nucleon on the lattice”. In: *Proceedings of Science LATTICE2019* (2020), p. 040. DOI: 10.22323/1.363.0040. arXiv: 1911.05051 [hep-lat].
- [2] J. Liang. “Hadronic Tensor and Neutrino-Nucleon Scattering”. In: *Proceedings of Science LATTICE2019* (2020), p. 046. DOI: 10.22323/1.363.0046.
- [3] A. Portelli. “Electromagnetic corrections to leptonic decays”. In: *Proceedings of Science LATTICE2019* (2020), p. 085. DOI: 10.22323/1.363.0085.
- [4] H. Ohki. “Computing Nucleon Electric Dipole Moment from lattice QCD”. In: *Proceedings of Science LATTICE2019* (2020), p. 290. DOI: 10.22323/1.363.0290.
- [5] Y. Zhao. “Theoretical Developments of the LaMET Approach to Parton Physics”. In: *Proceedings of Science LATTICE2019* (2020), p. 267. DOI: 10.22323/1.363.0267.
- [6] N. Karthik. “Developments in lattice computation of parton distributions”. In: *Proceedings of Science LATTICE2019* (2020), p. 277. DOI: 10.22323/1.363.0277.
- [7] Gunnar S. Bali et al. “Hyperon couplings from $N_f = 2 + 1$ lattice QCD”. In: *Proceedings of Science LATTICE2019* (2020), p. 099. DOI: 10.22323/1.363.0099. arXiv: 1907.13454 [hep-lat].
- [8] Y. Aoki et al. on behalf of the PACS Collaboration. “Proton decay matrix elements with physical quark masses”. In: *Proceedings of Science LATTICE2019* (2020), p. 141. DOI: 10.22323/1.363.0141.
- [9] S. Aoki et al. (Flavour Lattice Averaging Group). “FLAG Review 2019”. In: *European Physics Journal C* 80.2 (2020), p. 113. DOI: 10.1140/epjc/s10052-019-7354-7. arXiv: 1902.08191 [hep-lat].
- [10] Nesreen Hasan et al. “Nucleon axial, scalar, and tensor charges using lattice QCD at the physical pion mass”. In: *Physical Review D* 99.11 (2019), p. 114505. DOI: 10.1103/PhysRevD.99.114505. arXiv: 1903.06487 [hep-lat].

- [11] S. Ohta on behalf of the LHP, RBC, and UKQCD Collaborations. “Nucleon isovector charges from physical mass domain-wall QCD”. In: *Proceedings of Science LATTICE2019* (2020), p. 051. DOI: 10.22323/1.363.0051. arXiv: 1910.13860 [hep-lat].
- [12] A. Walker-Loud. “Callat elastic nucleon structure, 1”. In: *Proceedings of Science LATTICE2019* (2020), p. 257. DOI: 10.22323/1.363.0257.
- [13] Tim Harris et al. “Nucleon isovector charges and twist-2 matrix elements with $N_f = 2 + 1$ dynamical Wilson quarks”. In: *Physical Review D*100.3 (2019), p. 034513. DOI: 10.1103/PhysRevD.100.034513. arXiv: 1905.01291 [hep-lat].
- [14] O. Baer. “ $N\pi$ excited state contamination in nucleon 3-pt functions using ChPT”. In: *Proceedings of Science LATTICE2019* (2020), p. 078. DOI: 10.22323/1.363.0078.
- [15] C. Alexandrou et al. *The nucleon axial, tensor and scalar charges and σ -terms in lattice QCD*. 2019. arXiv: 1909.00485 [hep-lat].
- [16] N. Tsukamoto et al. “Nucleon isovector couplings from 2+1 flavor lattice QCD at the physical point”. In: *Proceedings of Science LATTICE2019* (2020), p. 132. DOI: 10.22323/1.363.0132. arXiv: 1912.00654 [hep-lat].
- [17] S. Park et al. “Nucleon charges and form factors using clover and HISQ ensembles”. In: *Proceedings of Science LATTICE2019* (2000), p. 136. DOI: 10.22323/1.363.0136. arXiv: 2002.02147 [hep-lat].
- [18] Huey-Wen Lin et al. “Quark contribution to the proton spin from 2+1+1-flavor lattice QCD”. In: *Phys. Rev. D*98.9 (2018), p. 094512. DOI: 10.1103/PhysRevD.98.094512. arXiv: 1806.10604 [hep-lat].
- [19] D. Djukanovic et al. “Strange nucleon form factors and isoscalar charges with $N_f = 2 + 1$ $O(a)$ -improved Wilson fermions”. In: *Proceedings of Science LATTICE2019* (2020), p. 158. DOI: 10.22323/1.363.0158. arXiv: 1911.01177 [hep-lat].
- [20] L. Varnhorst. “Nucleon Sigma Terms”. In: *Proceedings of Science LATTICE2019* (2000), p. 214. DOI: 10.22323/1.363.0214.
- [21] Yong-Chull Jang et al. “Nucleon electromagnetic form factors in the continuum limit from (2+1+1)-flavor lattice QCD”. In: *Physical Review D*101.1 (2020), p. 014507. DOI: 10.1103/PhysRevD.101.014507. arXiv: 1906.07217 [hep-lat].
- [22] Eigo Shintani et al. “Nucleon form factors and root-mean-square radii on a $(10.8 \text{ fm})^4$ lattice at the physical point”. In: *Physical Review D*99.1 (2019), p. 014510. DOI: 10.1103/PhysRevD.99.014510. arXiv: 1811.07292 [hep-lat].
- [23] C. Alexandrou et al. “Proton and neutron electromagnetic form factors from lattice QCD”. In: *Physical Review D*100.1 (2019), p. 014509. DOI: 10.1103/PhysRevD.100.014509. arXiv: 1812.10311 [hep-lat].
- [24] Veronique Bernard, Latifa Elouadrhiri, and Ulf-G. Meissner. “Axial structure of the nucleon: Topical Review”. In: *Journal of Physics G*28 (2002), R1–R35. DOI: 10.1088/0954-3899/28/1/201. arXiv: hep-ph/0107088 [hep-ph].

- [25] Aaron S. Meyer et al. “Deuterium target data for precision neutrino-nucleus cross sections”. In: *Physical Review D* 93.11 (2016), p. 113015. DOI: 10.1103/PhysRevD.93.113015. arXiv: 1603.03048 [hep-ph].
- [26] R. A. Smith and E. J. Moniz. “NEUTRINO REACTIONS ON NUCLEAR TARGETS”. In: *Nuclear Physics B* 43 (1972), p. 605. DOI: 10.1016/0550-3213(72)90040-5.
- [27] R. A. Smith and E. J. Moniz. “Erratum: NEUTRINO REACTIONS ON NUCLEAR TARGETS”. In: *Nuclear Physics B* 101 (1975), p. 547. DOI: 10.1016/0550-3213(75)90612-4.
- [28] A. A. Aguilar-Arevalo et al. (MiniBooNE). “First Measurement of the Muon Neutrino Charged Current Quasielastic Double Differential Cross Section”. In: *Physical Review D* 81 (2010), p. 092005. DOI: 10.1103/PhysRevD.81.092005. arXiv: 1002.2680 [hep-ex].
- [29] Rajan Gupta et al. “Axial Vector Form Factors of the Nucleon from Lattice QCD”. In: *Phys. Rev. D* 96.11 (2017), p. 114503. DOI: 10.1103/PhysRevD.96.114503. arXiv: 1705.06834 [hep-lat].
- [30] Constantia Alexandrou et al. “Nucleon axial form factors using $N_f = 2$ twisted mass fermions with a physical value of the pion mass”. In: *Physical Review D* 96.5 (2017), p. 054507. DOI: 10.1103/PhysRevD.96.054507. arXiv: 1705.03399 [hep-lat].
- [31] Yong-Chull Jang et al. “Axial Vector Form Factors from Lattice QCD that Satisfy the PCAC Relation”. In: *Physical Review Letters* 124.7 (2020), p. 072002. DOI: 10.1103/PhysRevLett.124.072002. arXiv: 1905.06470 [hep-lat].
- [32] G. S. Bali et al. “Solving the PCAC puzzle for nucleon axial and pseudoscalar form factors”. In: *Physics Letters B* 789 (2019), pp. 666–674. DOI: 10.1016/j.physletb.2018.12.053. arXiv: 1810.05569 [hep-lat].
- [33] Y.C. Jang et al. “Nucleon Axial Form Factors from Clover Fermion on 2+1+1-flavor HISQ Lattice”. In: *Proceedings of Science LATTICE2019* (2000), p. 131. DOI: 10.22323/1.363.0131. arXiv: 2001.11592 [hep-lat].
- [34] B. Yoon et al. “Neutron Electric Dipole Moments with Clover Fermions”. In: *Proceedings of Science LATTICE2019* (2000), p. 243. DOI: 10.22323/1.363.0243.
- [35] P. E. Shanahan and W. Detmold. “Gluon gravitational form factors of the nucleon and the pion from lattice QCD”. In: *Physical Review D* 99.1 (2019), p. 014511. DOI: 10.1103/PhysRevD.99.014511. arXiv: 1810.04626 [hep-lat].
- [36] P. E. Shanahan and W. Detmold. “Pressure Distribution and Shear Forces inside the Proton”. In: *Physical Review Letters* 122.7 (2019), p. 072003. DOI: 10.1103/PhysRevLett.122.072003. arXiv: 1810.07589 [nucl-th].
- [37] Ryan Bignell et al. “Neutron magnetic polarizability with Landau mode operators”. In: *Physical Review D* 98.3 (2018), p. 034504. DOI: 10.1103/PhysRevD.98.034504. arXiv: 1804.06574 [hep-lat].